Journal of Biomedical Optics

BiomedicalOptics.SPIEDigitalLibrary.org

Monitoring the progression from intraductal carcinoma to invasive ductal carcinoma based on multiphoton microscopy

Yan Wu
Fangmeng Fu
Yuane Lian
Yuting Nie
Shuangmu Zhuo
Chuan Wang
Jianxin Chen

SPIE.

Monitoring the progression from intraductal carcinoma to invasive ductal carcinoma based on multiphoton microscopy

Yan Wu,[a,b,†] Fangmeng Fu,[c,†] Yuane Lian,[d,†] Yuting Nie,[a] Shuangmu Zhuo,[a] Chuan Wang,[c,*] and Jianxin Chen[a,*]
[a]Fujian Normal University, Institute of Laser and Optoelectronics Technology, Fujian Provincial Key Laboratory for Photonics Technology, Key Laboratory of OptoElectronic Science and Technology for Medicine of Ministry of Education, No. 8, Shangsan Road, Cangshan, Fuzhou 350007, China
[b]Jimei University, School of Science, No. 185, Yinjiang Road, Jimei, Xiamen 361021, China
[c]Affiliated Union Hospital of Fujian Medical University, Department of Breast Surgery, No. 29, Xinquan Road, Gulou, Fuzhou 350001, China
[d]Affiliated Union Hospital of Fujian Medical University, Department of Pathology, No. 29, Xinquan Road, Gulou, Fuzhou 350001, China

Abstract. Intraductal carcinoma is a precancerous lesion of the breast and the immediate precursor of invasive ductal carcinoma. Multiphoton microscopy (MPM) was used to monitor the progression from intraductal carcinoma to invasive ductal carcinoma, which can improve early detection of precursor lesions and halt progression to invasive neoplastic disease. It was found that MPM has the capability to reveal the qualitative changes in features of cells, structure of basement membranes, and architecture of collagens during the development from intraductal carcinoma to invasive ductal carcinoma, as well as the quantitative alterations in nuclear area, circle length of basement membrane, and collagen density. Combined with intra-fiberoptic ductoscopy or transdermal biopsy needle, MPM has the potential to provide immediate histological diagnosis of tumor progression in the field of breast carcinoma. [DOI: 10.1117/1.JBO.20.9.096007]

Keywords: multiphoton microscopy; mammary ductal carcinoma; tumor progression; monitoring.

Paper 150315PR received May 11, 2015; accepted for publication Jul. 20, 2015; published online Sep. 10, 2015.

1 Introduction

Breast cancer is the second leading cause of cancer-related deaths in women and accounts for approximately one-third of all cancers diagnosed among women in the United States, with an estimated 234,190 new cases and 40,730 deaths in 2015.[1] Most breast cancers originate from epithelium, and mammary ductal carcinoma is the most common type, which involves two main forms: intraductal carcinoma and invasive ductal carcinoma. It is generally accepted by the scientific and medical communities that intraductal carcinoma is a precancerous lesion of the breast and the immediate precursor of invasive ductal carcinoma.[2,3] Thus, monitoring the progression from intraductal carcinoma to invasive ductal carcinoma can improve early detection of precursor lesions and halt progression to invasive neoplastic disease. Currently used imaging modalities for precursor lesions diagnosis and breast cancer screening, including x-ray mammography, breast ultrasonography, and magnetic resonance imaging (MRI), are limited to resolutions of 1 mm. However, for understanding the progression of breast cancer, a much higher spatial resolution (1 μm or less) is required to visualize structural changes associated with cells and tissues, and observe the interaction between tumor cells and extracellular matrix. Thus, the ability to observe cellular details and provide real-time pathological diagnosis of tumor staging during tumor progression is a major goal in the development of advanced breast imaging techniques.

In this context, several optical imaging techniques, such as optical coherence tomography (OCT), Raman spectroscopy, laser scanning confocal microscopy (LSCM), and multiphoton microscopy (MPM), have been developed. Among these, OCT provides full-thickness, high-resolution, cross-sectional images, but cannot distinguish biological constituents;[4] Raman spectroscopy can identify disease lesions by capturing intrinsic chemical changes within tissues, but is limited by its long acquisition time (>1 s/pixel) for high spatial resolution, preventing its applications from fast scanning of a large surface area;[5] LSCM is a useful biomedical tool, but has phototoxicity problems resulting from its ultraviolet light source.[6] In contrast, MPM based on two-photon excited fluorescence (TPEF) and second-harmonic generation (SHG) offers significant advantages for imaging thick tissue and live animals, including enhanced axial depth discrimination, enhanced penetration depth in scattering samples, and reduced overall specimen photodamage and photobleaching, because it uses a near-infrared light source.[7]

Given the advantages provided by MPM, it has been widely applied to visualize cellular morphology and stromal architecture in breast tissue without the use of exogenous contrast agents.[8–10] The previous publications have shown that in breast tissue, TPEF is well suited for high-resolution imaging of intrinsic molecular signals from elastin and cells, while SHG enables direct imaging of anisotropic biological structures of collagen. In this work, we take advantage of MPM to simultaneously perform *ex vivo* TPEF imaging of cancer cells and SHG imaging of stroma in different stages during tumor progression, including normal mammary duct, intraductal carcinoma, and invasive

*Address all correspondence to: Chuan Wang, E-mail: chuanwang1968@hotmail.com; Jianxin Chen, E-mail: chenjianxin@fjnu.edu.cn

†These authors contributed equally to this work.

1083-3668/2015/$25.00

ductal carcinoma, and obtain quantitative data not possible with confocal microscopy or other imaging modalities. It is of great significance to image and quantify the cellular and stromal alterations involved in disease progression under *ex vivo* conditions for further using MPM to perform *in vivo* investigations of tumor progression in clinic.

2 Materials and Methods

2.1 *Sample Preparation*

A total of 14 patients (aged 32 to 66 years) with mammary ductal carcinoma were recruited to participate in this study, which was approved by the institutional review board of the Affiliated Union Hospital, Fujian Medical University, and conformed with the institutional rules governing clinical investigations of human subjects in biomedical research. Written informed consent was obtained prior to study participation. After removal by surgeons, each specimen was placed in a standard pathologic transport container, covered with ice, and then sent to a pathology laboratory. Every specimen was cut into five serial slices ~10 μm thick by cryostat microtome. The middle slice was stained with hematoxylin and eosin (H&E) for histological images and the remaining sections were for multiphoton microscopic imaging. In order to compare mammary ductal lesions with normal tissue, a total of five fresh biopsy specimens were obtained from patients without mammary ductal lesions, as is normally the case.

2.2 *Multiphoton Microscopic Imaging System*

The MPM system has been described previously.[11] Briefly, a commercial LSM 510 META (Zeiss, Jena, Germany) equipped with a mode-locked femtosecond Ti:sapphire laser (110 fs, 76 MHz) operating at 810 nm (Coherent Mira 900-F) was utilized to obtain high-resolution images of normal and ductal cancerous breast tissues. A high numerical aperture, oil-immersion objective (Plan-Apochromat 63×, N.A. 1.4, Zeiss) was employed for focusing the excitation beam into tissue samples and was also used to collect the backscattered intrinsic SHG and TPEF signals. The signals were directed by a main dichroic beam splitter to the META detector. The META detector consisted of a high-quality reflective grating and an optimized 32-channel photomultiplier tube (PMT) array, covering a spectral width of ~340 nm ranging from 377 to 716 nm and a single PMT covering a spectral range of 10.7 nm. An IR beam block filter (Zeiss KP650) in front of the META detector was used to ensure that excitation light was filtered out and only emission signals were recorded. In this work, the multichannel mode, which has eight independent channels where each channel can selectively be set to detect emission signals within the random range from 377 to 716 nm, was used to achieve TPEF/SHG imaging.

2.3 *Imaging Acquisition*

For multiphoton microscopic imaging, the tissue section on the slide glass was first sprinkled with a small amount of phosphate buffered saline to avoid dehydration or shrinkage, then covered by a coverslip and sealed with nail polish, and finally imaged with the coverslip facing the microscope objective. In this work, one channel covering the wavelength range from 430 to 716 nm and the other channel covering the wavelength range from 389 to 419 nm were properly set to collect the TPEF and SHG signals, respectively. The specific system parameters of these two independent channels were listed in Table 1. In order to increase the contrast of the TPEF/SHG image, the TPEF images were color-coded in red and SHG images were color-coded in green. Large-area images were achieved by translating the samples using an optional HRZ 200 fine focusing stage (HRZ 200 stage, Carl Zeiss). All images had a 12-bit pixel depth. The images were obtained at 2.56 μs per pixel.

Table 1 System parameters of two independent channels.

Channels	Detector gain	Amplifier offset	Amplifier gain	Laser power (mw)
Second-harmonic generation (SHG)	759	0	1	3.8
Two-photon excited fluorescence (TPEF)	742	−0.17	1	6.4

2.4 *Imaging Analyses*

MPM images were qualitatively analyzed by two experienced individuals to identify different stages during mammary ductal carcinoma progression and then confirmed by comparison with H&E images, which were obtained using a standard bright field light microscope (Eclipse Ci-L, Nikon Instruments Inc., Japan) with a CCD (Nikon, DS-Fi2, Japan) and reviewed by a certified pathologist.

After qualitative analysis, the nuclear area, circle length of basement membrane, and collagen density were quantitatively calculated to characterize morphological changes associated with mammary ductal carcinoma progression. The nuclear area was calculated by measuring the area enclosed by the nuclear boundary. The circle length of the basement membrane was obtained by measuring the length of the basement membrane's outline. Collagen density was defined as the ratio of SHG to all pixels in each image, which was taken from collagen bundles in the stroma surrounding normal or affected ducts, or in the stroma invaded by cancer cells. Each quantitative analysis was performed on all samples.

Summary statistic for nuclear area, circle length of basement membrane, and collagen density arose from normal breast tissue ($n = 25$ areas of 5 samples), intraductal carcinoma ($n = 30$ areas of 6 samples), and invasive ductal carcinoma ($n = 40$ areas of 8 samples). Data were expressed in the form of a mean value followed by its standard deviation (mean $\pm$ SD); the standard deviation signified the change of every feature parameter. One-way analyses of variance were conducted to compare differences using SPSS (version 15.0), and differences were considered to be statistically significant when $p < 0.05$.

3 Results

Most breast carcinomas develop in the terminal duct lobular unit.[12,13] Figure 1 shows representative TPEF/SHG images and the corresponding H&E stained image of a normal mammary duct. The TPEF image [Fig. 1(a)] reveals the appearance of a mammary duct with a central oval to round lumen (position 1), which is lined by epithelial cells (white arrows). The epithelial cells have bright cytoplasm based on the TPEF signals of cellular nicotinamide adenine dinucleotide hydrogen (NADH) and flavin adenine dinucleotide (FAD), and a dark nucleus because of its nonfluorescence.[14] Mammary ducts are surrounded by dense connective tissues, which are mostly

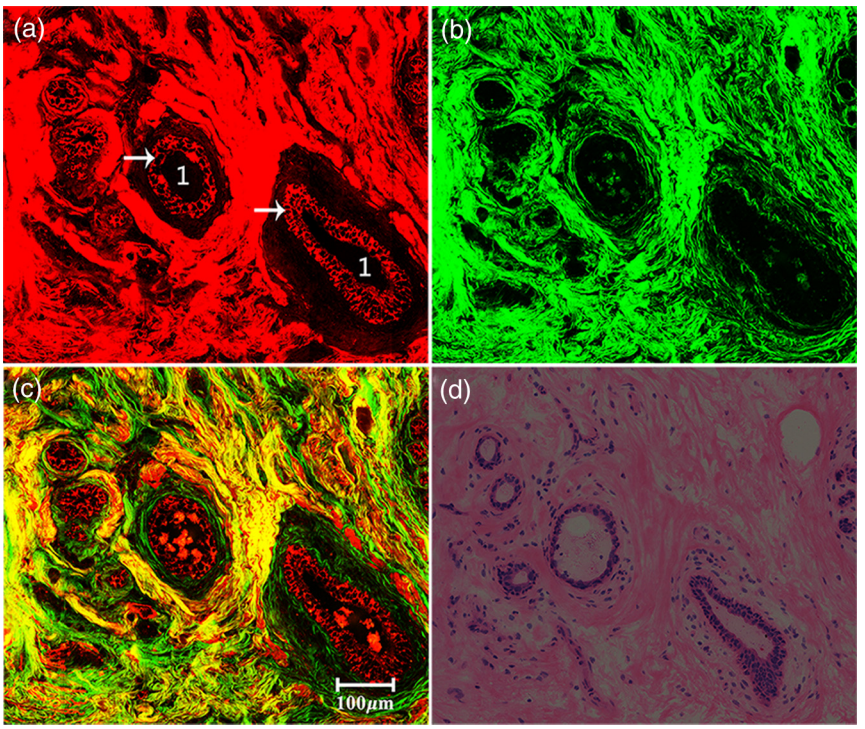

Fig. 1 Representative two-photon excited fluorescence (TPEF)/second-harmonic generation (SHG) images and corresponding H&E stained image of normal breast tissue. (a) TPEF image of collagen and epithelial cells (color-coded red), (b) SHG image of collagen (color-coded green), (c) the overlaid image of TPEF and SHG, and (d) the corresponding H&E stained image (magnification, 40×). Position 1: ductal lumen; white arrows: epithelial cells.

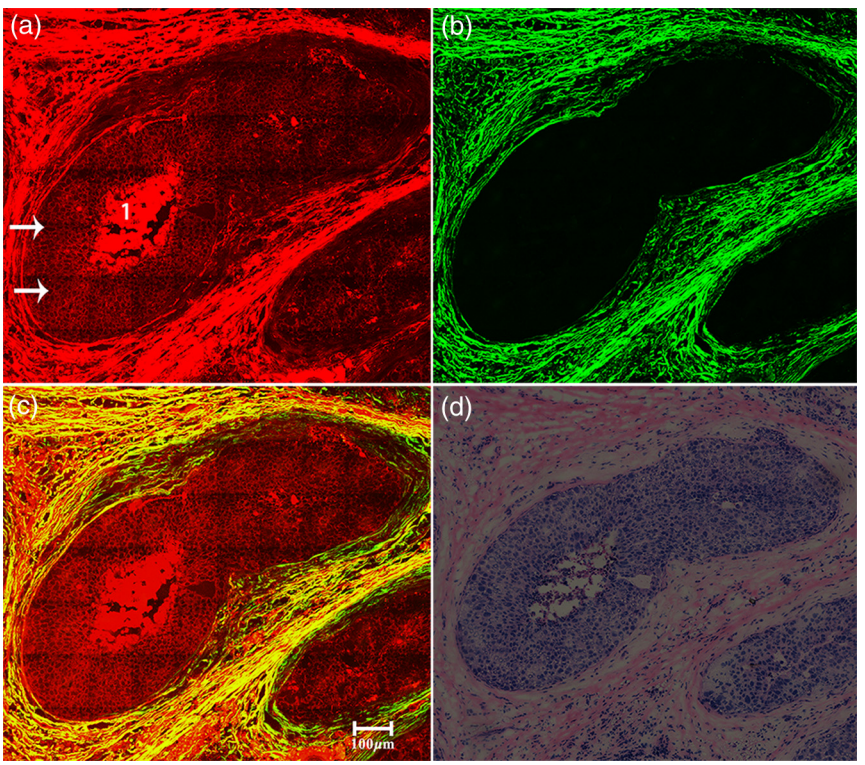

Fig. 2 Representative TPEF/SHG images and corresponding H&E stained image of intraductal carcinoma. (a) TPEF image of carcinomatous cells, necrosis, and collagen (color-coded red), (b) SHG image of collagen (color-coded green), (c) the overlaid image of TPEF and SHG, and (d) the corresponding H&E stained image (magnification, 40×). Position 1: intraluminal necrosis; white arrows: malignant cells.

composed of collagen bundles. The SHG image [Fig. 1(b)] shows that collagen is thick with the morphology of fine mesh.[15] In the high-contrast overlaid TPEF/SHG image [Fig. 1(c)], collagens turn yellowish because they have comparable TPEF and SHG signals.[16] In addition, the basement membrane of the duct is also clearly identified because of the strong SHG signals generated by collagen fibers.[17] All these microstructures of the mammary duct and surrounding collagen readily correlate with the H&E stained image [Fig. 1(d)].

While the abnormal cells have not moved out of the mammary duct and into any of the surrounding tissues in the breast, breast neoplasm is often referred to as intraductal carcinoma. Figure 2 displays representative TPEF/SHG images and the corresponding H&E stained image of intraductal carcinoma. Unlike a normal case, malignant epithelial cells (white arrows) obviously enlarge, distinctly proliferate, and almost fill the duct, which leads to the loss of hollow lumen [Fig. 2(a)]. Remarkably, intraluminal necrosis can be clearly identified in the TPEF image (position 1), which is an important character in the pathological grading of intraductal carcinoma.[18,19] Collagen bundles show no significant alteration, and the basement membranes were relatively well preserved, but presented a distorted structure with a larger size [Fig. 2(b)]. These observations were consistent with the results of previous publications and also confirm the fact that proliferated cells are confined to the ductal system and do not destroy the basement membrane at the precancerous stages.[20] The high-contrast overlaid image of TPEF and SHG clearly displays the microstructure of intraductal carcinoma [Fig. 2(c)]. These qualitative morphological variations are in excellent agreement with the paired histopathological sections with H&E staining [Fig. 2(d)].

Unlike intraductal carcinoma, invasive ductal carcinoma involves invasion of the primary tumor into surrounding tissue by penetrating the basement membrane of the mammary duct.[20] Figure 3 shows representative TPEF/SHG images and the corresponding H&E stained image of invasive ductal carcinoma. Compared to normal breast tissue, malignant cells (white arrows) invade into the surrounding stroma and arrange in small clusters (position 1) [Fig. 3(a)]. Moreover, they are larger and more nonuniform than normal epithelial cells. During tumor progression, the basement membranes are destroyed and finally disappear in invasive ductal carcinoma [Fig. 3(b)]. The collagen bundles obviously display a significant loss because many abnormal cells infiltrate and displace their locations through degrading collagen [Fig. 3(b)]. In addition, they are significantly thinner and are randomly oriented with greater bundle spacing. The high-contrast overlaid image of TPEF and SHG clearly displays the microstructure of invasive ductal carcinoma [Fig. 3(c)]. These qualitative morphological variations are also in excellent agreement with the paired histopathological sections with H&E staining [Fig. 3(d)].

Not only well-defined samples as shown in Figs. 1–3, but also not-so-well-defined samples can be identified by MPM. Figure 4 shows the representative TPEF/SHG image of invasive

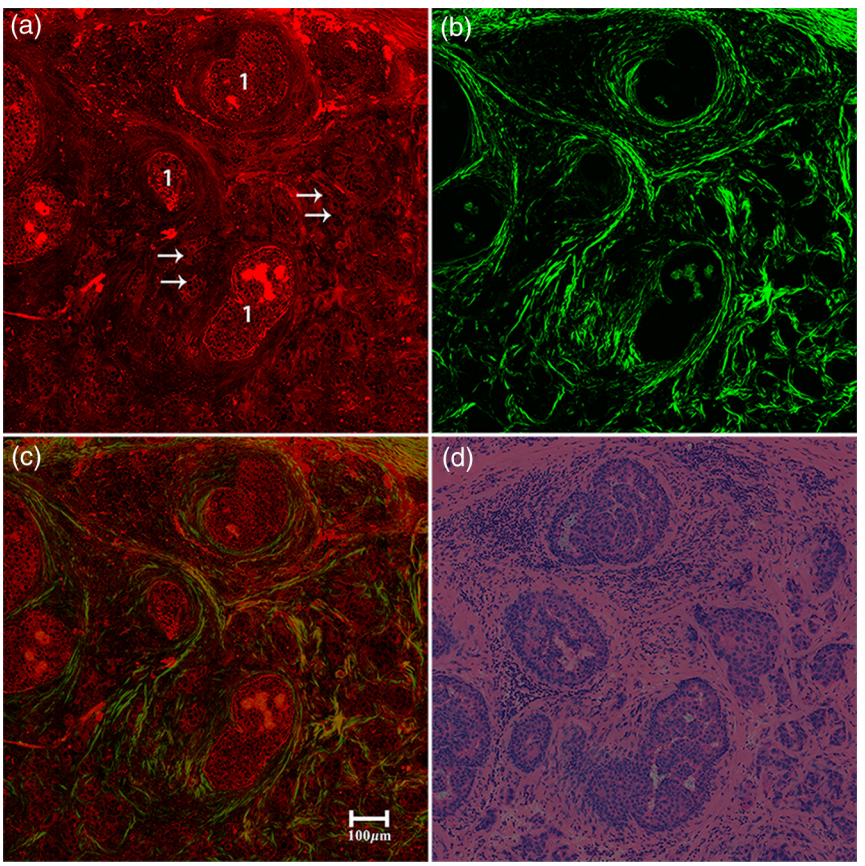

Fig. 3 Representative TPEF/SHG images and corresponding H&E stained image of invasive ductal carcinoma. (a) TPEF image of carcinomatous cells and collagen (color-coded red), (b) SHG image of collagen (color-coded green), (c) the overlaid image of TPEF and SHG, and (d) the corresponding H&E stained image (magnification, 40×). Position 1: clusters of cancer cells; white arrows: malignant cells.

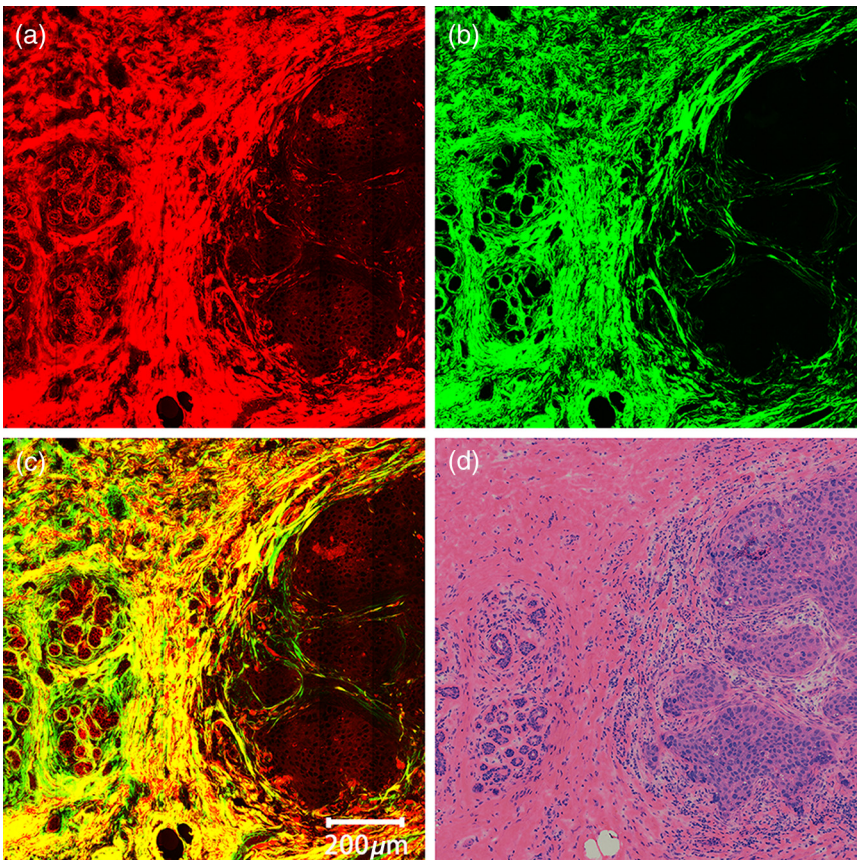

Fig. 4 Representative TPEF/SHG images and corresponding H&E stained image of invasive ductal carcinoma invading into surrounding healthy tissue. (a) TPEF image of normal and carcinomatous cells and collagen (color-coded red), (b) SHG image of collagen (color-coded green), (c) the overlaid image of TPEF and SHG, and (d) the corresponding H&E stained image (magnification, 40×).

ductal carcinoma invading into surrounding healthy tissue. The overall TPEF/SHG image [Fig. 4(c)] can be divided into two parts. In the left part, TPEF/SHG image evidently displays the microstructure of breast tissue without invasion of cancer cells. Ducts are lined by simple columnar epithelia and obvious basement membrane, and collagen bundles in stroma are dense with the morphology of fine mesh, which are similar to that seen in normal breast tissue. In the right part, the TPEF/SHG image clearly reveals the infiltrative growth pattern of invasive ductal carcinoma, which is characterized by a sheet or areatus structure. Unlike what is observed in the left part, tumor cells invade into the surrounding tissue with enlarged nucleus and collagen bundles become thinner and more fractured. The boundary between these two parts is readily discerned due to the completely different spatial arrangements of normal and tumor cells and collagen bundles. The same details of the cellular feature and stromal architecture correlate readily with the H&E stained image [Fig. 4(d)].

Figure 5 shows the representative TPEF/SHG image of evolution from intraductal carcinoma to invasive ductal carcinoma. Two enlarged ducts, which are filled with tumor cells and intraluminal necrosis, are conspicuous in Fig. 5(a), indicated by white arrows. Furthermore, basement membranes can also be seen clearly [red arrows in Fig. 5(b)], which become thinner and nearly disappear for facilitating the invasion of tumor cells. This demonstrates that the breast tissue is undergoing evolution from intraductal carcinoma to invasive ductal carcinoma. Moreover, invasive tumor cells are also identified by MPM, indicated by "position 1" in Fig. 5(c). The fact that intraductal carcinoma and invasive ductal carcinoma affect the same anatomical site here further illustrates that they are progressive stages of an evolutionary continuum. The same details of the cellular feature and stromal architecture correlate readily with the H&E stained image [Fig. 5(d)].

Comparison of the TPEF/SHG image of a normal mammary duct with intraductal and invasive ductal carcinoma clearly shows that MPM has the ability to identify different stages during the development of mammary ductal carcinoma. As illustrated by Table 2, the features of cells, structure of basement membranes, and architecture of collagens are all important characters in identifying tumor staging. Thus, in order to quantitatively describe the tumor progression, nuclear area, circle length of basement membrane, and collagen density are calculated and their detailed information are summarized in Table 3. Quantitative results reveal that the nuclear area obviously increases and presents a larger standard deviation in intraductal and invasive ductal carcinoma compared to normal epithelial cells. The circle length of basement membrane continuously increases with the stepwise progression of mammary ductal carcinoma and defines as "∞" when basement membranes disappear in the final stage. Collagen density shows an obvious loss in invasive ductal carcinoma compared to the normal case and the precursor lesion. Then one-way analyses of variance are conducted to compare differences using SPSS software (version

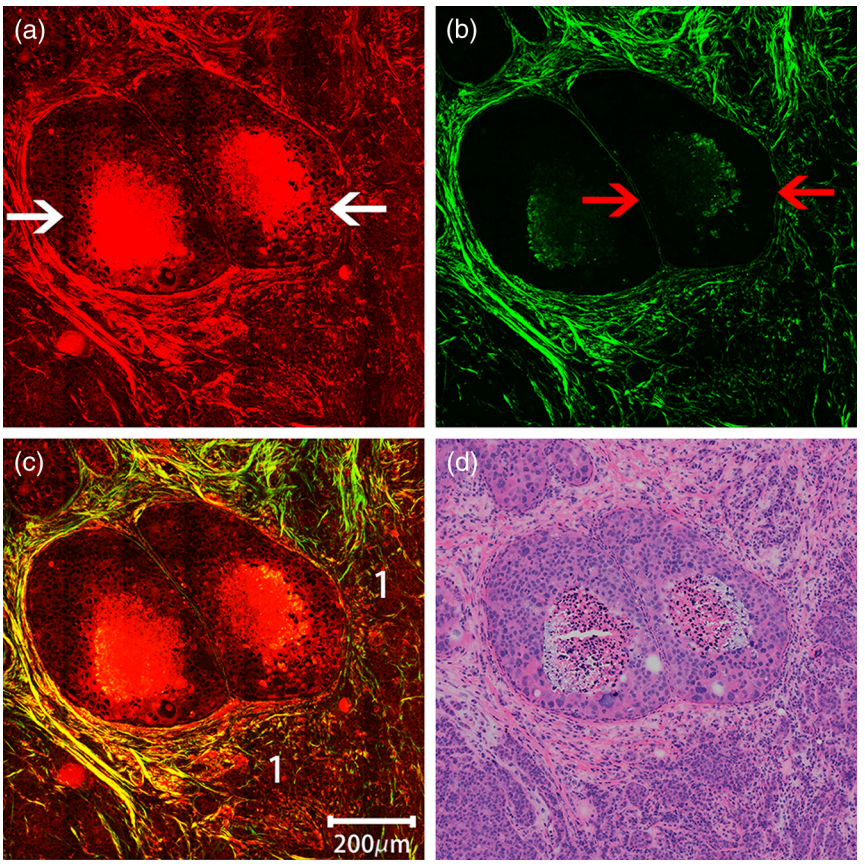

Fig. 5 Representative TPEF/SHG images and corresponding H&E stained image of evolution from intraductal carcinoma to invasive ductal carcinoma. (a) TPEF image of carcinomatous cells, necrosis, and collagen (color-coded red), (b) SHG image of collagen (color-coded green), (c) the overlaid image of TPEF and SHG, and (d) the corresponding H&E stained image (magnification, 40×). White arrows: enlarged ducts; red arrows: thin basement membranes; position 1: invasive cancerous cells.

Table 2 Multiphoton microscopy (MPM) identification of mammary ductal carcinoma progression according to cellular feature, structure of basement membrane, and architecture of collagen.

Tissue	Cellular feature based on TPEF image	Structure of basement membrane based on SHG imaging	Architecture of collagen based on SHG imaging
Normal duct	• Cell arranging along basement membrane	• Basement membrane with round shape generating strong SHG signals	• Collagen organizing in an aligned fashion with the morphology of fine mesh
	• Nuclei with round shape and uniform size		• Collagen being thick with small bundle spacing
Intraductal carcinoma	• Cell proliferating and almost filling the duct	• Basement membrane being relatively well preserved but presenting the distorted structure with a larger size	• Collagen showing no significant alteration in comparison with normal case
	• Increased nuclear area		
Invasive ductal carcinoma	• Cell invading into stroma and arranging in small cluster	• Basement membranes being destroyed and finally disappearing	• Collagen displaying a significant loss and arranging randomly
	• Further increased nuclear area		• Collagen being thin with greater bundle spacing

15.0); differences are considered to be statistically significant when the p values are <0.05. The representative example of quantitative analysis and the summary of statistics are represented in Fig. 6.

Based on MPM identified features established in Tables 2 and 3, MPM is used to diagnose 19 samples obtained from patients recruited in this paper. The result of MPM diagnosis compared with H&E histopathology has been shown in Table 4,

Table 3 Quantitative morphological features in different stages during mammary ductal carcinoma progression.

Morphological feature	Normal case	Intraductal carcinoma	Invasive ductal carcinoma
Nuclear area (μm^2)	23.72 ± 4.99	110.67 ± 40.89	103.86 ± 23.44
Circle length of basement membrane (μm)	189.58 ± 56.32	1263.33 ± 1016.83	∞
Collagen density	0.62 ± 0.13	0.60 ± 0.18	0.19 ± 0.12

which shows that the accuracy, sensitivity, and specificity of MPM in diagnosis of breast cancer and normal breast tissue are 94.74% $[(8+5+5)/19]$, 92.86% $[(8+5)/14]$, and 100% (5/5), respectively. Furthermore, MPM is also highly sensitive and highly accurate for diagnosis of tumor staging including intraductal carcinoma and invasive ductal carcinoma. The discrepancy in MPM and H&E comparison is only shown in one sample of well-differentiated ductal carcinoma in situ, which is diagnosed as a normal case. In this work, every specimen is cut into five serial slices, among which four sections are used for MPM imaging. Therefore, the MPM imaging of each sample is repeated four times to ensure the robustness of the test, and the results show that MPM diagnoses are all in excellent agreement for each sample. The number of patients recruited in this study for the accuracy and robustness test is limited because it is difficult to recruit more volunteers; however, it does not affect the conclusion that MPM has the potential to

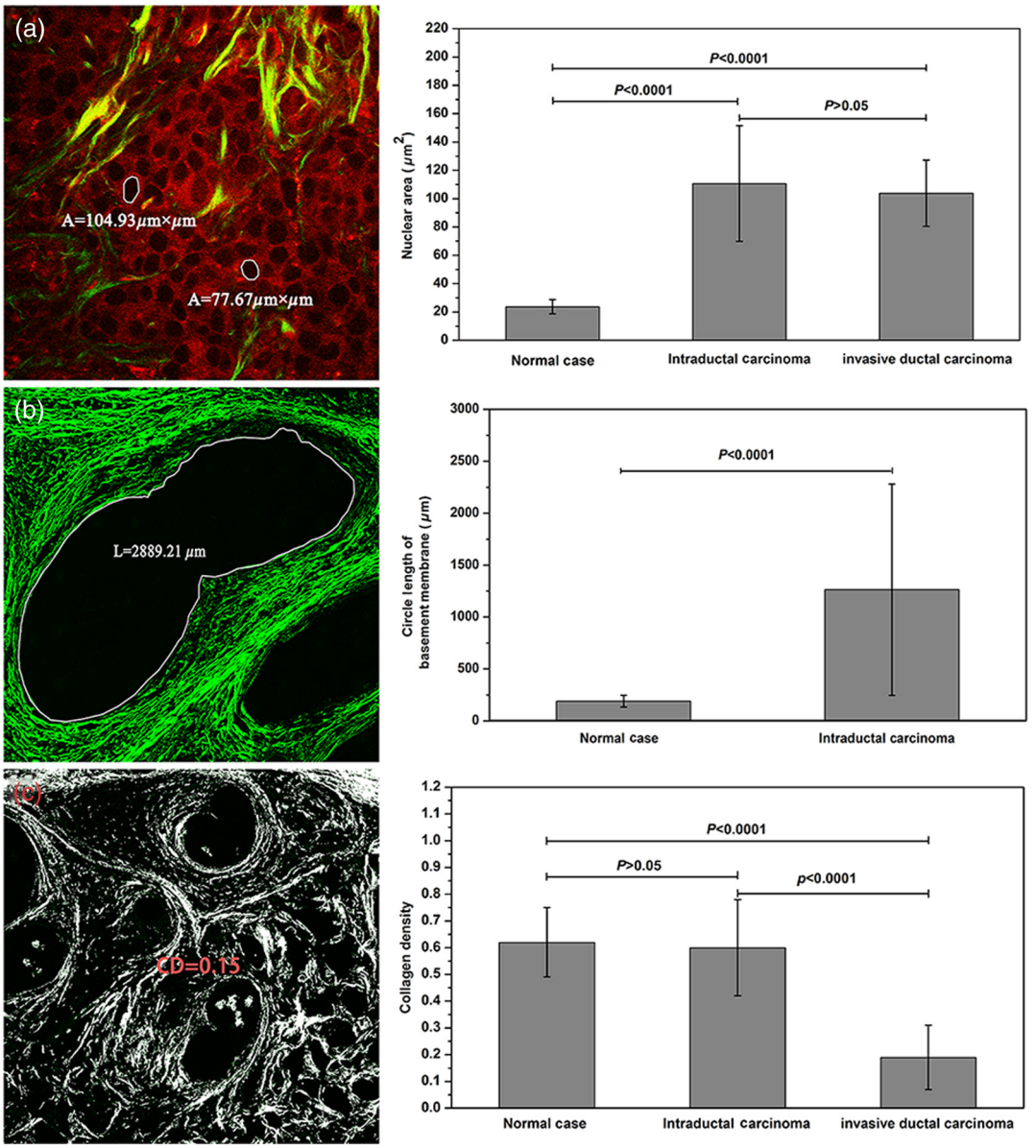

Fig. 6 Representative quantitative example and summary statistics of (a) nuclear area, (b) circle length of basement membrane, and (c) collagen density. A, L, and CD are the abbreviations for nuclear area, circle length of basement membrane, and collagen density, respectively.

Table 4 Comparing MPM diagnosis of cancer staging with H&E diagnosis.

$N = 19$		H&E diagnosis		
		Invasive ductal carcinoma ($N1 = 8$)	Intraductal carcinoma ($N2 = 6$)	Normal case ($N3 = 5$)
MPM diagnosis	Invasive ductal carcinoma ($N4 = 8$)	8	0	0
	Intraductal carcinoma ($N5 = 5$)	0	5	0
	Normal case ($N6 = 6$)	0	1	5

provide immediate diagnosis of tumor progression, comparable to histopathology. In addition, MPM diagnosis is time-efficient, which is a great advantage of MPM over traditional histopathology. For example, a routine histopathological procedure, including formalin fixation, dehydration, paraffin embedding, slicing, and H&E staining, may takes three to five days, but MPM diagnosis can be achieved within a few hours.

4 Discussion

In 1973, Wellings proposed that nonmalignant ductal lesions are precursors of invasive breast cancer based on the evidence of gradual histological continuity observed in normal and abnormal breast tissues.[21] Clinical observational studies further corroborate the hypothesis that intraductal carcinoma and invasive breast cancer are progressive stages of an evolutionary continuum by the evidence that they affect the same anatomical site.[22] It is important to investigate the epithelial and stromal alterations involved in disease progression to determine those precursors likely to progress to malignancy and, therefore, to provide individualized treatment to patients with intraductal carcinoma. However, there is currently no validated medical imaging technique that can visualize mammary epithelium and stroma at the molecular level to accurately predict the progression of mammary ductal carcinoma.

MPM has become one of the most important optical imaging techniques for biomedical research by excitation of tissue-intrinsic fluorescent molecules, which provides a superior effective resolution in comparison with confocal microscopy. In this paper, our study has shown that NADH and FAD in epithelial cells and necrosis can generate strong TPEF signals, collagen fibers in basement membrane of intraductal carcinoma can emit strong SHG signals, and collagen bundles in stroma have comparable TPEF and SHG signals. Based on the TPEF and SHG signals of these intrinsic fluorescent molecules, MPM can not only reveal changes in the morphology of epithelial cells, but also identify alterations in the features of basement membrane and the architecture of stroma during mammary ductal carcinoma progression. In addition, MPM can also quantitatively describe the change of the nuclear area, circle length of the basement membrane, and collagen density, establishing a quantitative link between these pathological features and mammary ductal carcinoma progression. All these qualitative variations and quantitative analyses correspond well to the paired histopathological sections with H&E staining, demonstrating that MPM has the potential to provide real-time histological diagnosis of tumor progression.

MPM has tremendous potential in terms of clinical application, and the transformation of MPM into the clinics has been performed. First, researchers have developed several miniature multiphoton endoscopy and flexible MPM probes with small diameters for imaging internal organs of small animals in a minimally invasive fashion.[23–26] Brown et al. first demonstrated that *in vivo* images of unstained liver, kidney, and colon from an anesthetized rat can be achieved by using a compact and flexible multiphoton microendoscope.[23,24] Yan et al. have implemented *in vivo* dynamic fluorescence microendoscopic imaging and monitored the movement of blood flow beneath the skin in anesthetized mice, using a fluorescence endoscopic imaging system based on gradient index (GRIN) lenses.[26] Second, the invention of new photonic crystal fibers allows fiber delivery of 100-fs pulses through optical fibers with more than enough power for MPM imaging, which makes it possible for physicians or surgeons to directly deliver high-resolution imaging to the pathology lab.[27,28] Last, mapping an MPM image into pseudo-H&E colors can display structures and colors analogous to H&E staining, which facilitates pathologists to make histopathological diagnoses.[29] All of these suggest that MPM has the potential to provide *in vivo* diagnosis of breast cancer progression.

Compared to other tissues, breast is much more superficial and particularly accessible with the MPM technique. Along with MPM probes, GRIN lenses, and photonic crystal fibers, MPM can be integrated into the intra-fiberoptic ductoscopy or transdermal biopsy needle, which will allow to provide immediate *in vivo* diagnosis of tumor progression, avoiding repeated needle or surgical biopsies, reducing patient anxiety while waiting on the results, and expediting the scheduling of procedures in cases of carcinoma.[17] Once MPM serves as an advanced breast imaging technology for clinical applications like x-ray mammography, breast ultrasonography, MRI, and fiberoptic ductoscopy, assessing the tumor progression will probably become its main application in the field of breast carcinoma. This study provides the groundwork for the further use of MPM to perform such real-time noninvasive diagnosis of tumor progression in mammary ductal carcinoma.

5 Conclusion

In conclusion, MPM can be used to monitor the progression from intraductal carcinoma to invasive ductal carcinoma according to morphological changes in epithelial cells, basement membrane, and collagen-rich stroma, and qualitative alterations in nuclear area, circle length of basement membrane, and collagen density. With the development and clinical applications of MPM probes, GRIN lenses, and photonic crystal fibers, real-time *in vivo* evaluation of tumor progression may become its main application of MPM in the field of breast cancer. This will be useful for the early detection of precursor lesions and halting its progression to invasive neoplastic disease.

Acknowledgments

The project was supported by the Program for Changjiang Scholars and Innovative Research Team in University (Grant No. IRT1115), the National Natural Science Foundation of China (Grant No. 81271620), the Natural Science Foundation for Distinguished Young Scholars of Fujian Province (Grant No. 2014J06016), and the Program for Training Young and

Middle-aged Backbone Talents in Healthy System of Fujian Province (Grant No. 2013-ZQN-ZD-12).

References

1. R. L. Siegel, K. D. Miller, and A. Jemal, "Cancer statistics, 2015," *CA: Cancer J. Clin.* **65**, 5–29 (2015).
2. D. C. Allred et al., "Histological and biological evolution of human premalignant breast disease," *Endocr. Relat. Cancer* **8**, 47–61 (2001).
3. G. S. Dalgin et al., "Portraits of breast cancer progression," *BMC Bioinf.* **8**, 291 (2007).
4. S. C. Whiteman et al., "Optical coherence tomography: real-time imaging of bronchial airways microstructure and detection of inflammatory/neoplastic morphologic changes," *Clin. Cancer Res.* **12**, 813–818 (2006).
5. A. S. Haka et al., "Diagnosing breast cancer by using Raman spectroscopy," *PNAS* **102**, 12371–12376 (2005).
6. P. T. C. So, Y. D. Chen, and R. M. Barry, "Two-photon excitation fluorescence microscopy," *Annu. Rev. Biomed. Eng.* **2**, 399–429 (2000).
7. W. R. Zipfel, R. M. Williams, and W. W. Webb, "Nonlinear magic: multiphoton microscopy in the biosciences," *Nat. Biotechnol.* **21**, 1369–1377 (2003).
8. A. Zoumi, A. Yeh, and B. J. Tromberg, "Imaging cells and extracellular matrix in vivo by using second-harmonic generation and two-photon excited fluorescence," *Proc. Natl. Acad. Sci.* **99**, 11014–11019 (2002).
9. P. P. Provenzano et al., "Nonlinear optical imaging of cellular processes in breast cancer," *Microsc. Microanal.* **14**, 532–548 (2008).
10. P. P. Provenzano et al., "Nonlinear optical imaging and spectral-lifetime computational analysis of endogenous and exogenous fluorophores in breast cancer," *J. Biomed. Opt.* **13**, 031220 (2008).
11. S. Zhuo et al., "Multimode nonlinear optical imaging of the dermis in ex vivo human skin based on the combination of multichannel mode and Lambda mode," *Opt. Express* **14**, 7810–7820 (2006).
12. M. C. Pike et al., "Estrogens, progestogens, normal breast cell proliferation, and breast cancer risk," *Epidemiol. Rev.* **15**, 17–35 (1993).
13. J. D. Figueroa et al., "Terminal duct lobular unit involution of the normal breast: implications for breast cancer etiology," *JNCI J. Natl. Cancer Inst.* **106**, dju286 (2014).
14. J. Chen et al., "Establishing diagnostic features for identifying the mucosa and submucosa of normal and cancerous gastric tissues by multiphoton microscopy," *Gastrointest. Endosc.* **73**, 802–807 (2011).
15. G. Falzon, S. Pearson, and R. Murison, "Analysis of collagen fibre shape changes in breast cancer," *Phys. Med. Biol.* **53**, 6641–6652 (2008).
16. J. Chen et al., "Spectroscopic characterization and microscopic imaging of extracted and in situ cutaneous collagen and elastic tissue components under two-photon excitation," *Skin Res. Technol.* **15**, 418–426 (2009).
17. X. Wu et al., "Label-free detection of breast masses using multiphoton microscopy," *PLoS One* **8**, e65933 (2013).
18. J. S. Meyer, "Cell kinetics of histologic variants of in situ breast carcinoma," *Breast Cancer Res. Treat.* **7**, 171–180 (1986).
19. G. F. Schwartz, "The role of excision and surveillance alone in subclinical DCIS of the breast," *Oncology (Williston Park)* **8**, 21–26 (1994).
20. K. Burke, P. Tang, and E. Brown, "Second harmonic generation reveals matrix alterations during breast tumor progression," *J. Biomed. Opt.* **18**, 031106 (2013).
21. S. R. Wellings and H. M. Jensen, "On the origin and progression of ductal carcinoma in the human breast," *J. Natl. Cancer Inst.* **50**, 1111–1118 (1973).
22. C. F. Cowell et al., "Progression from ductal carcinoma in situ to invasive breast cancer: revisited," *Mol. Oncol.* **7**, 859–869 (2013).
23. C. M. Brown et al., "In vivo imaging of unstained tissues using a compact and flexible multiphoton microendoscope," *J. Biomed. Opt.* **17**, 040505 (2012).
24. D. M. Huland et al., "In vivo imaging of unstained tissues using long gradient index lens multiphoton endoscopic systems," *Biomed. Opt. Express* **3**, 1077–1085 (2012).
25. D. Kobat, N. G. Horton, and C. Xu, "In vivo two-photon microscopy to 1.6-mm depth in mouse cortex," *J. Biomed. Opt.* **16**, 106014 (2011).
26. W. Yan et al., "Fluorescence microendoscopy imaging based on GRIN lenses with one- and two-photon excitation modes," *Front. Optoelectron.* **8**, 177–182 (2015).
27. D. G. Ouzounov et al., "Delivery of nanojoule femtosecond pulses through large-core microstructured fibers," *Opt. Lett.* **27**, 1513–1515 (2002).
28. X. Zhu et al., "Monitoring wound healing of elastic cartilage using multiphoton microscopy," *Osteoarthritis Cartilage* **21**, 1799–1806 (2013).
29. Y. K. Tao et al., "Assessment of breast pathologies using nonlinear microscopy," *Proc. Natl. Acad. Sci.* **111**, 15304–15309 (2014).

Yan Wu received her MS degree in condensed matter physics in 2007 from Xiamen University, China. She is working at Jimei University, Xiamen, China. She is now working toward her PhD in optics at Fujian Normal University, China. Her main research interests are focused on nonlinear spectroscopy and biomedical imaging.

Fangmeng Fu is now working in the Department of Breast Surgery, Affiliated Union Hospital of Fujian Medical University, majoring in surgical therapy of breast cancer. His main research interests are focused on the genetics and pharmacogenomics of breast cancer.

Yuane Lian, received her MS degree in pathology in 2011 from Fujian Medical University, China. She is now working in the Department of Pathology, Affiliated Union Hospital of Fujian Medical University. Her main research interests are focused on the pathology of breast cancer.

Yuting Nie received her BS degree in physics in 2012 from Shangrao Normal University, China. She is currently working toward her MS degree in optical engineering at Fujian Normal University, China. Her main research interests are focused on nonlinear optical imaging.

Shuangmu Zhuo received his PhD in optics engineering from Fujian Normal University, China, in 2012. He then joined the Singapore-MIT Alliance for Research and Technology as a postdoctoral research fellow. He is currently an associate professor in the College of Photonic and Electronic Engineering, Fujian Normal University, China. His research interests include the development and applications of nonlinear optical microscopy and biomedical research.

Chuan Wang is now working in the Department of Breast Surgery, Affiliated Union Hospital of Fujian Medical University, majoring in surgical therapy of breast cancer. His main research interests are focused on the genetics and pharmacogenomics of breast cancer.

Jianxin Chen is a professor and director of the Key Laboratory of Optoelectronic Science and Technology for Medicine of Ministry of Education and vice secretary general of the Chinese Optical Society. Her research areas are the application of depth-resolved nonlinear spectral imaging for determining the pathology of epithelial tissue based on two-photon excited autofluorescence and second-harmonic generation and application of multimode nonlinear optical imaging for evaluating physiological and pathological states of tissues.